Synthetic Biology for Vector-Borne Diseases

K. Sneppen*
Niels Bohr Institute, University of Copenhagen, Blegdamsvej 17, DK-2100 Copenhagen, Denmark

I. Østerlund
Department of Plant and Environmental Sciences, University of Copenhagen, Copenhagen, Thorvaldsensvej 40, 1871 Frederiksberg C, Denmark

S. L. Svenningsen
Department of Biology, University of Copenhagen, Copenhagen, Ole Maaløes Vej 5, 2200 København N, Denmark

S. Brown
Niels Bohr Institute, University of Copenhagen, Copenhagen, Denmark

(Received 22 May 2023; accepted 8 August 2023; published 14 September 2023)

Safe experimentation addressing the spread of epidemic disease requires extreme care. Risks can be avoided through the development of model systems where analogs of epidemic processes can be manipulated in the laboratory and compared with predictions from mathematical models. Here we describe an integrated mathematical and experimental analysis of a vector-borne disease. The experimental system we developed, "malaria in a Petri dish," requires alternating host bacteria to propagate a dimorphic virus. Unlike typical vector-borne diseases, this model system uses only nonhazardous and inexpensive materials. We quantified the growth properties of the hosts and viral forms and examined the spread of the virus between independent bacterial microcolonies in an immobilized suspension. The combined model and experiment found the spatial constraints imposed by alternating microcolony infections strongly inhibited the spread of the disease. Our mathematical model allowed us to mimic the propagation of the infections and predicted how propagation increased when the spatial heterogeneity was decreased. The model also correctly predicted the efficiency of herd immunity when immunizing a fraction of the bacterial population.

DOI: 10.1103/PRXLife.1.013015

I. INTRODUCTION

Vector-borne diseases play a substantial role in public health. The World Health Organization estimates more than one-sixth of human infections are due to vector-borne diseases causing more than 700 000 deaths annually [1]. Vector-borne diseases can be caused by bacteria, viruses, or parasites. Transmission of a vector-borne disease to humans is mediated by a second host, called a vector, which is most often a bloodsucking insect. Vector-borne diseases include such classic horrors as malaria, sleeping sickness, dengue, and yellow fever. Vector-borne diseases continue to emerge as, for example, Lyme disease (reviewed in [2]). In the case of malaria, dengue, and yellow fever, the vector hosts are mosquitoes. Tsetse flies are the vector hosts of sleeping sickness, while ticks are the vector host for Lyme disease.

To examine the spread of a vector-borne disease, we developed a model system based on two viruses that infect the bacterium *Escherichia coli*, bacteriophages (phages) λ and M13. The model system allowed us to not only examine the spread of this vector-borne disease but to examine the effects of partial immunization and spatial separation between the two host types.

Phages λ and M13 display several properties that allow them to emulate vector-borne disease. They bind to different surface features of *E. coli* in order to infect. These surface features can be removed by mutation. Both phages are temperate; that is, they can persistently infect their hosts without killing the host bacteria. Furthermore, they are well-characterized, nonhazardous model systems whose genetics can be easily manipulated.

Phage λ is a double-stranded DNA virus whose wild-type genome length is 48 514 base pairs [3]. It recognizes the *E. coli* surface protein, LamB, which is part of the *E. coli* maltose-utilization system [4,5]. M13 is a filamentous single-stranded DNA virus whose wild-type genome length is 6407 nucleotides [6]. M13 recognizes the *E. coli* surface structure, the F-pilus (reviewed in [7]). The F-pilus is part of a bacterial gene transfer system that requires cell-cell contact. Neither the maltose-utilization system nor the F (or fertility) factor are required for growth of *E. coli* under most conditions. Therefore, strains of *E. coli* can be constructed that permit entry of only one and not the other phage.

When wild-type λ infects a sensitive *E. coli*, the phage can enter one of two developmental pathways (reviewed in

*ksneppen@gmail.com

[8]). The infecting phage can enter lytic development where the host produces on the order of 100 progeny phages that are released by lysis of the infected bacterium. Alternatively, the infecting phage can enter lysogenic development where it represses most of its genes and integrates its genome into the *E. coli* chromosome. In the lysogenic state it produces a cytoplasmic protein, the λ repressor. The λ repressor is the product of the λ *cI* gene and prevents lytic development of not only the resident prophage but also of superinfecting λ phages. That is, the lysogen is immune to superinfection by λ.

The single-stranded M13 genome is made double stranded upon infection of the host and replicates in the cytoplasm. M13 does not lyse the host to release progeny phages; instead the host secretes progeny phages without killing the bacterium [7]. Wild-type M13 encodes both its DNA replication system and the structural proteins of the phage capsid in its genome. However, only a small portion of the M13 genome, the intergenic (IG) region, is necessary to direct a circular DNA molecule to produce a single-stranded circle that will be encapsidated and secreted [9]. The rest of the necessary M13 genes must be in the same bacterial cell but can reside on a different DNA molecule. M13 development is not inhibited by the λ repressor.

II. RESULTS

A. The dimorphic bacteriophage

We prepared a dimorphic bacteriophage, λS3243, starting with materials used to make large [10] DNA origami [11]. The dimorphic bacteriophage could be produced in two forms depending on the host bacterium it infects (Fig. 1).

λS3243 contains the following features in its 48 892-base-pair genome: Most of its genome is that of wild-type λ. The genome also contains a ColE1 origin of replication that will allow it to replicate as a double-stranded circle on infecting a λ-immune host. It also encodes a thermolabile form of the λ repressor, CI857, which will enter λ lytic development when infecting a sensitive host at elevated temperatures. However, it retains sensitivity to the wild-type λ repressor and will not enter λ development when infecting a host containing the wild-type λ repressor. It contains the M13 IG region that will allow it to be replicated by the M13 replication system [12] producing a single-stranded, circular DNA (see Fig. S1 of the Supplemental Material [13]). The circular, single-stranded DNA is packaged and secreted in an M13 form if the host encodes all of the M13 proteins. Last, it contains the gene for green fluorescent protein (GFP), *gfp*, under control of the regulatable *lac* operator. Infected bacteria will fluoresce green when excited with the correct wavelength of light, making it possible to track the infection by monitoring GFP fluorescence. Construction of λS3243 is described in Materials and Methods.

These features of λS3243 make it possible to emulate a vector-borne disease by choosing a suitable pair of host strains. These are strains of *E. coli* that are only susceptible to infection by the phage form produced by the other host strain and are unable to be infected by the phage form produced by their own type.

B. Two hosts

If λS3243 infects a bacterium whose cytoplasm does not contain the λ repressor it develops like phage λ and packages

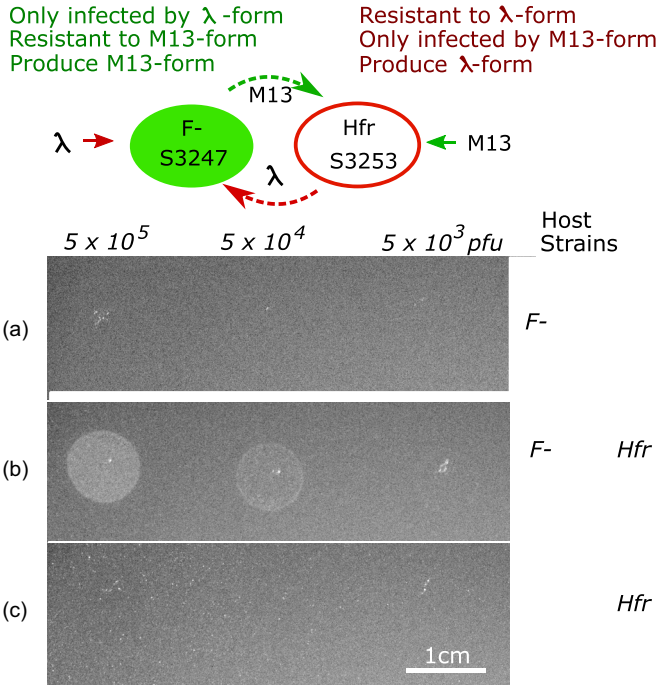

FIG. 1. Top: Schematic summarizing the two-host requirement for spread of the dimorphic phage. Bottom [(a)–(c)]: Lawn with *E. coli* strain(s) exposed to the λ form of the phage. Green fluorescence is shown. Top agar in panels (a) and (b) contained S3247, an F^- strain that can be infected by the λ form and produce the M13 form. Top agar in panels (b) and (c) contained S3253, an Hfr strain that can be infected by the M13 form and produce the λ form of phage. Both strains are $lacI^-$ and could express GFP if infected. Panels (a)–(c) show that both F^- and Hfr strains were needed to observe green fluorescence. The values on the top refer to the number of λ-form plaque-forming units (PFU) used to initialize infection. Bacteria were used at our standard concentrations (see text).

double-stranded DNA with cohesive ends into λ phage particles. If grown on a λ-immune host harboring an M13 helper plasmid, it produces an approximately 6-micron-long M13 based on genome lengths and length of wild-type M13 phage [14]. The M13 helper plasmid we used, pSB4423, contains all the genes of M13 but lacks the M13 origin of DNA replication [10]. The λ form requires LamB, the λ receptor, for infection. The gene encoding the λ receptor is deleted with Δ*malB101*. The M13 form requires the F-pilus for infection. When the F plasmid is integrated into the bacterial chromosome the strain is designated Hfr. Properties of host strains are summarized in Table I and Materials and Methods.

C. Both host types are necessary for the infection to spread

The upper panel of Fig. 1 illustrates why both host types must be present for the infection to spread. Only the λ developmental pathway, not the M13 developmental pathway, of λS3243 is repressed by the wild-type λ repressor expressed from the host chromosome. S3247 infected with λS3243 therefore continues to grow, producing both GFP and progeny viruses in its M13 form. The M13-form progeny cannot directly infect S3247 as this strain lacks the F-pilus necessary for M13 infection. However, the M13 form can infect the Hfr

TABLE I. Summary of the behaviors of the hosts after infection at 37 °C with λS3243. The parentheses for GFP refers to a transient signal because the bacteria lyse upon infection. The strains used in this study and the preparation of the dimorphic bacteriophage are described in Materials and Methods.

Strain	Infected by λ form	Infected by M13 form	Post-infected state	Progeny phages	GFP produced
KS3	−	+	lives	none	+
KS5	+	−	lives	none	+
S3247	+	−	lives	M13 form	+
S3248	+	−	lives	M13 form	−
S3249	−	+	dies	λ form	(−)
S3253	−	+	dies	λ form	(+)

strain, here S3253. This strain does not support production of the M13 form because it lacks the genes encoding M13 proteins. Upon infection of S3253, the λ form begins development, leading to subsequent release of progeny phages in their λ form. The *gfp* gene of λS3243 can be transcribed in S3253, but after lysis accompanying release of the λ form, GFP will no longer be localized. S3253 cannot be infected directly by the λ form as it lacks the surface protein necessary for λ infection.

The requirement for both hosts is visualized experimentally in the lower portion of Fig. 1. A soft-agar overlay contained the F^- and/or the Hfr strain. The number of bacterial cells occupying each spot at our standard concentration was $\approx 1.2 \times 10^6$ for the F^- strains and 1.2×10^5 for the Hfr strains (9 mm diameter). The initial density of total bacteria was 3×10^7/ml in the top layer and 2×10^6/ml in terms of total agar (food availability). Dilutions of the λ form of λS3243 were spotted on top of the soft agar and the plates were incubated at 37 °C overnight. All experiments were conducted in a minimal-glycerol-casamino acids (MC) medium (Materials and Methods). GFP production was visualized using a 465-nm lamp and 520-nm long-pass filter. The green channel is illustrated in the figures, where GFP fluorescence from infected cells can be seen as a light zone. Fluorescence was only observed if both hosts were present Fig. 1(b)]. The fluorescence also varied with the concentration of added phage. The same conclusions were reached when infections were initiated with the M13 form (see Supplemental Material Figs. S2 and S3 [13]).

D. The fluorescence signal arises mainly from the F^- hosts

The promoter of *gfp* in λS3243 is regulated by the *lac* repressor. If the bacterial host produces the *lac* repressor, especially from the *lac* repressor overproduction allele, $lacI^Q$, the transcription of *gfp* from the infecting phage will be reduced. Conversely, if the bacterial host lacks the gene for the *lac* repressor, as when the entire *lac* operon is missing, Δ*lac*, the transcription of *gfp* from the infecting phage will be increased.

We used the Δ*lac* and $lacI^Q$ alleles to distinguish the GFP production of hosts that propagate the λ form from hosts that propagate the M13 form of λS3243 in mixed infections. Figure 2 illustrates our results. As in the experiment above, cultures of the indicated bacterial strains were dispersed in a soft-agar overlay and dilutions of λS3243 as either the λ form or the M13 form were spotted on the surface. After overnight growth at 37 °C fluorescence produced by GFP was visualized. Expression of GFP was observed if only the F^- host lacks the *lac* repressor. Expression of GFP was not observed if only the Hfr host lacks the *lac* repressor. GFP produced in the Hfr strain can diffuse away from the spot after cell lysis caused by the development of the λ form. Additional strain combinations can be seen in Supplemental Material Figs. S2 and S3 [13].

E. Immune hosts and single-cycle infections

The strategy to restrict phage propagation to a single cycle of infection is depicted in the left portion of Fig. 3. To restrict the propagation of the dimorphic phage to a single cycle we prepared two additional host strains, KS5 and KS3 (Table I and Materials and Methods). KS5, like S3247, can be infected only by the λ form of λS3243 but unlike S3247 produces no

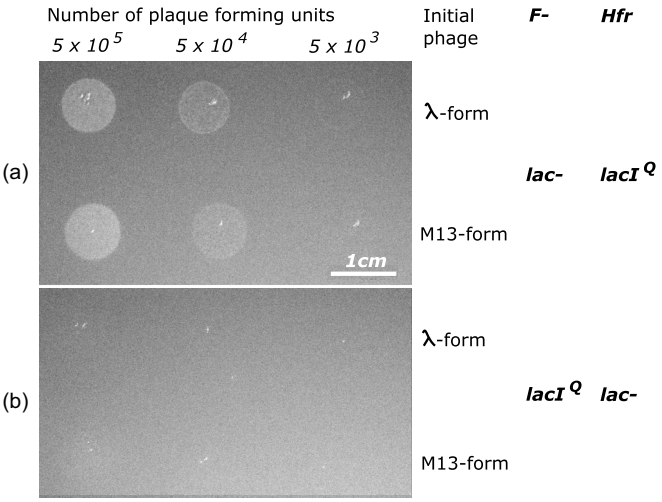

FIG. 2. Mixed lawn with two *E. coli* strains illustrating an initial infection with either of the phage types can give green spot, provided that the F^- strain can express GFP. (a) GFP expression if only the F^- strain was deleted for the *lac* repressor gene (here described as lac^-). The F^- strain was S3247 and the Hfr strain was S3249. (b) GFP expression if only the Hfr strain was deleted for the *lac* repressor gene (here described as lac^-). The F^- strain was S3248 and the Hfr strain was S3253. In the upper row of each panel the spots contained the λ form of the phage. In the lower rows of each panel are the spots with the M13 form. The plaque-forming units on the top refer to number of viable phages in each initial spot. Bacteria were used at our standard concentrations (Methods).

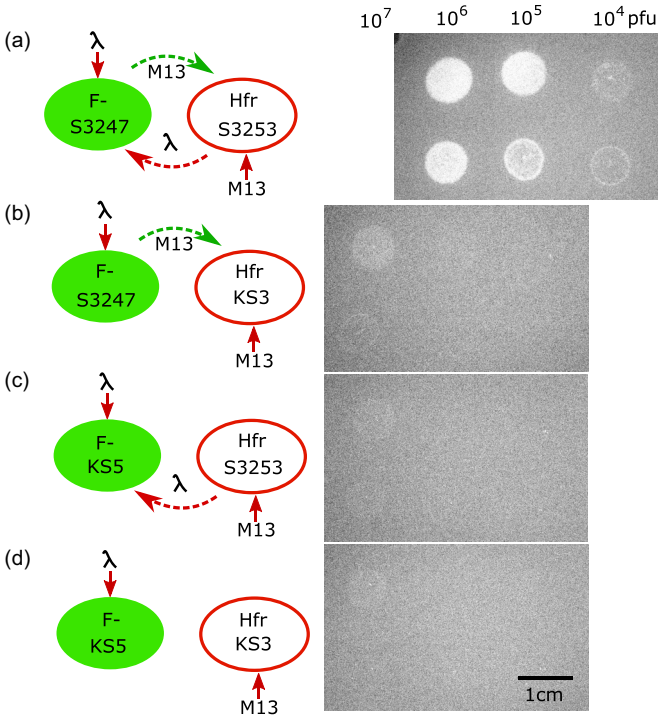

FIG. 3. Single-cycle experiments. We prepared a set of host strain pairs that could support (a) multiple cycles of infection or [(b), (c)] only a single cycle of infection. The permitted cycles are depicted in the left set of drawings. All hosts were *lacI*$^-$ and allow the phage-encoded GFP to be expressed. Bacteria were used at our standard concentrations (Methods). The number of phages as PFU per spot are cited above the right panels. The right panels are offset to accommodate the different numbers of phages necessary to observe fluorescence in the phage spots. The upper row of spots in each panel were initiated with the λ form of the dimorphic phage. The lower row of spots in each panel were initiated with the M13 form. The scale bar in (d) represents 1 cm and all panels are the same scale. Phage preparations in this experiment were fractionated with polyethylene glycol to remove contaminating GFP produced during phage growth ([15] and Supplemental Material [13]).

progeny, neither the λ nor the M13 form. Like S3247, KS5 is *lacI*$^-$ allowing the phage-encoded GFP to be expressed. KS3, like S3253, can be infected only by the M13 form but unlike S3253 produces no progeny, neither the λ nor the M13 form. Like S3253, KS3 is *lacI*$^-$ allowing the phage-encoded GFP to be expressed. Thus, if KS5 replaces S3247 or KS3 replaces S3253, only a single cycle of phage propagation can take place.

Fluorescence from the propagation of the dimorphic phage can be seen in Fig. 3. Figure 3(a) shows the fluorescence induced when multiple cycles of phage infection were permitted. When infected by only 10 000 plaque-forming units (PFU) of either form, the combination of S3247 and S3253 produced obvious fluorescence. In contrast, both single-cycle host pairs required at least a thousand times the number of input phage to generate the fluorescence produced with multiple cycles of phage propagation.

If S3253 was replaced with KS3, 10^7 PFU were necessary to produce a similar amount of fluorescence [compare Figs. 3(a) and 3(b)]. KS3 can be infected by the M13 form and produce GFP but cannot produce the λ form. It also cannot be infected with the λ form.

Similarly, if S3247 is replaced with KS5, 10^7 PFU of either form produced barely detectable fluorescence [Fig. 3(c)]. KS5 can be infected by the λ form and produce GFP but not progeny phages. KS5 lacks the F-pilus and cannot be infected by the M13 form. Both the bacteria in Fig. 3(d) can be infected and produce GFP but neither can produce progeny phages. In summary, on the order of 1000 times as many infectious phages were required to produce the same amount of GFP fluorescence if only a single cycle was permitted than if multiple cycles were permitted. The difference in fluorescence between Figs. 3(b) and 3(c) is likely due to a decreased copy number in absence of M13 helper in KS5 and thus failure of the infecting phage to replicate from the M13 origin [12].

Spots in Figs. 3(b)–3(d) with the highest number of phages were initiated with many more phage than available bacteria. Since these spots failed to produce bright fluorescence in the single-cycle hosts, continued reinfection must have been necessary to produce a strong fluorescence signal when multiple cycles were permitted.

F. Model

1. *Equations and parameters*

The top drawing in Fig. 1 outlines the microbial experimental system for a vector-borne disease consisting of two bacterial strains $f = \mathrm{F}^-$ and $v = \mathrm{Hfr}$ (v for vector) that are both essential for propagating the dimorphic phage. Here we model this system for bacteria suspended in top agar with food resources corresponding to the total volume of agar.

The λ form of the phage is quantified by its density P_λ and infects the $f = \mathrm{F}^-$ strain, leading to infected F^- host labeled f^*. These subsequently produce the M13 form measured in terms of concentration P_m. The M13 form of the phage infects the $v = \mathrm{Hfr}$ strain, leading to lysis and production of β_λ of the λ form. The standard approximation for well-mixed infections fails to fit the experimental data as it does not take into account that phages have to alternate between colonies of different types of bacteria. We here modify the equation to take into account adsorption to colonies of hosts [16]. The model is based on an extension of [16] that takes this requirement of alternating between the two colony types in each replication cycle. The equations for time development of f, $f*$, and P_m read

$$\frac{df}{dt} = \Gamma_f f\mathcal{C} - \eta_\lambda P_\lambda f_{\mathrm{avai}} + \Gamma_{\mathrm{cure}} f^*\mathcal{C}, \tag{1}$$

$$\frac{df_1}{dt} = \eta_\lambda P_\lambda f_{\mathrm{avai}} - f_1 \frac{n_m}{\tau_m} + \Gamma_f f_1 \mathcal{C}, \tag{2}$$

$$\frac{df_i}{dt} = f_{i-1}\frac{k_m}{\tau_m} - f_i \frac{k_m}{\tau_m} + \Gamma_f f_i \mathcal{C}, \quad i = 2, 3, \ldots, \tag{3}$$

$$\frac{df^*}{dt} = f_n \frac{k_m}{\tau_m} + \Gamma_f f^*\mathcal{C} - \Gamma_{\mathrm{cure}} f^*\mathcal{C}, \tag{4}$$

$$\frac{dP_m}{dt} = \Omega_m f^*\mathcal{C} - \eta_m P_m v_{\mathrm{abs}} - Loss_m P_m, \tag{5}$$

where we assume F^- cells grow in latency as λ development is repressed. Measurements of parameters for growth rates and phage production are quantified in Fig. 4 and tabulated in Table II. The limited resources are taken into account by $\mathcal{C} = 1 - (v + v^L + f + f^L + f^*)/K$, with capacity K.

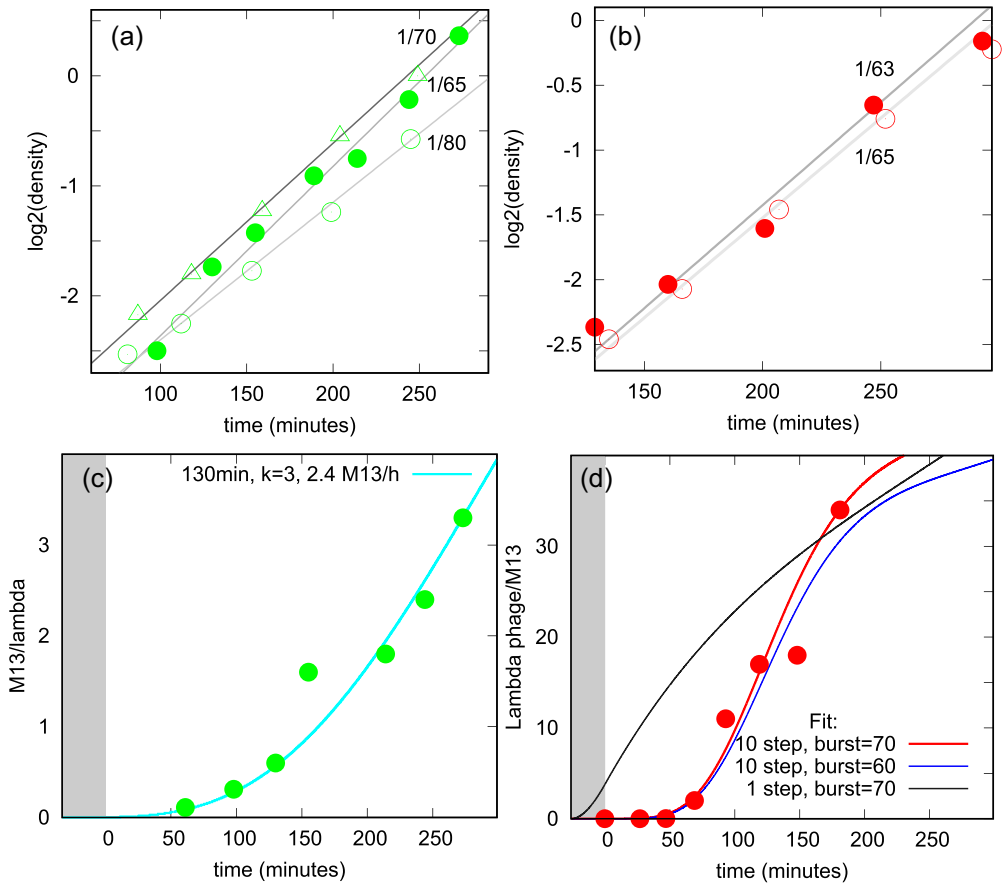

FIG. 4. Parameter estimations: Experimental data on bacterial growth after establishing steady state and phage production in MC broth (dots), and model fits represented with lines. (a) Growth of S3247, an F^- strain with helper for producing the M13 form ($\Gamma_f = \ln(2)/72$ min). (b) Growth of S3249, an Hfr strain for producing the λ form. Panels (a) and (b) each show independent experiments, defining F^- doubling to 72 min and Hfr doubling to 64 min. (c) Production of M13 form after infection of S3247 with λS3243. It is fitted by a 130-min latency with $k = 3$ steps, subsequent production of 2.4 M13/hour if curing rate $\Gamma_{\text{cure}} = 0.8\Gamma_f$. (d) Production of the λ form after infection of S3249 with the M13 form of λS3243. A 150-min latency with $k = 10$ steps and a burst $\beta = 70$ fit data. Experiments shown in panels (c) and (d) were each performed once. Experimental details are described in the Supplemental Material [13]. We also present alternative model fits, using exponentially distributed latency times ($k = 1$ step) or a different burst size. The grey areas in (c) and (d) mark incubation times after which the culture was diluted.

The concentrations $v^L = \sum_i v_i$ and $f^L = \sum_j f_j$ represent the respective hosts in latency states. At the end of the Supplemental Material [13] we show that the organization of f and v into colonies can be taken into account through the effective absorption and adsorption rates (Fig. S5):

$$v_{\text{abs}} = v_0\left(\frac{v+v^L}{v_0}\right)^{1/3},$$

$$v_{\text{avai}} = v_{\text{abs}}\exp\left(-\frac{\frac{v^L}{v_0}}{4\left(\frac{(v+v^L)}{v_0}\right)^{2/3}}\right),$$

$$f_{\text{abs}} = f_0\left(\frac{f+f^L+f^*}{f_0}\right)^{1/3},$$

$$f_{\text{avai}} = f_{\text{abs}}\exp\left(-\frac{\frac{(f^L+f^*)}{v_0}}{4\left(\frac{(f+f^L+f^*)}{v_0}\right)^{2/3}}\right).$$

This represents phage access to bacteria that are assigned to two types of spherical colonies, each of which contains a number of bacteria determined by dividing the current host density by the initial host densities of respectively $f = f_0$ and $v = v_0$. Here the total absorption to colonies is set by f_{abs} and v_{abs} dependent on type of colony. Given that a phage is adsorbed to the colony, the chance to be adsorbed to an uninfected cell is estimated by assuming that already-infected host cells are randomly distributed on the surface of the colonies. The exponential distribution used in calculating available susceptible hosts v_{avai} and f_{avai} comes from calculating the chance to encounter a noninfected cell on the surface of a spherical colony with a number of bacteria given by $(v + v^L)/v_0$ and $(f + f^L + f^*)/f_0$, respectively.

The equations for production and decay of P_λ are

$$\frac{dv}{dt} = \Gamma v\mathcal{C} - \eta_m P_m v_{\text{avai}}, \tag{6}$$

$$\frac{dv_1}{dt} = \eta_m P_m v_{\text{avai}} - v_1\frac{k_\lambda}{\tau_\lambda}, \tag{7}$$

$$\frac{dv_i}{dt} = v_{i-1}\frac{k_\lambda}{\tau_\lambda} - v_i\frac{k_\lambda}{\tau_\lambda} \quad \text{for } i = 2, 3, \ldots, n_\lambda, \tag{8}$$

$$\frac{dP_\lambda}{dt} = \beta\mathcal{C}v_{n_\lambda}\frac{k_\lambda}{\tau_\lambda} - \eta_\lambda P_\lambda f_{\text{abs}} - Loss \times P_\lambda, \tag{9}$$

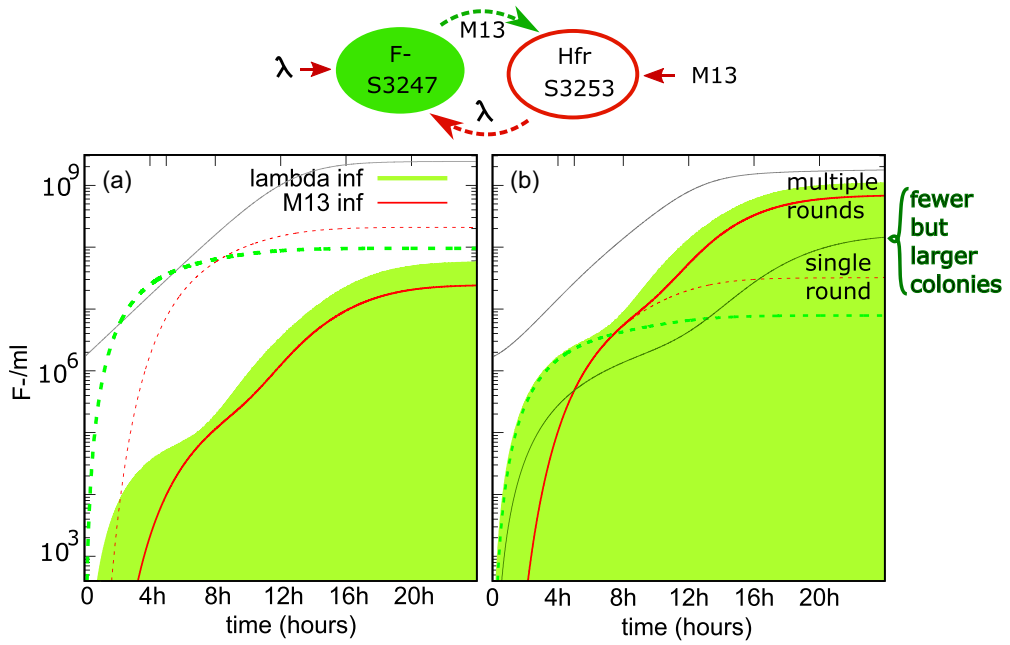

FIG. 5. Simulations of model with figures showing infected F^- and grey curve marking the population of uninfected F^-. All cases start with a mixed lawn of 2×10^6/ml *E. coli* partitioned in 91% F^- and 9% Hfr. (a) Green areas mimic a spot infection of 10.000 λ-form phages. Dashed lines model a lawn that only permits a single cycle but with an initial phage load that is 1000-fold higher [mimicking the leftmost case in Figs. 3(b) and 3(c)]. (b) Simulations started with 0.7×10^6 PFU/spot of either the λ form or the M13 form [compare to Fig. 2(a)]. Dashed curves mark single-cycle simulations at the same starting conditions. The dark green solid curve marks simulations with ten times lower initial bacterial density.

where we assume that the infected Hfr host does not grow during the latency period for development of the λ form [17].

Most of the parameters are fitted to appropriate measurements of bacteria growth as culture turbidity (A600 or absorbance at 600 nm) measurements, and phage yield as PFU (see Fig. 5). Parameters are listed in Table II.

We also consider the effect of partial immunization. This is implemented by assigning a fraction of host cells able to adsorb phages but does not produce progeny phages. In simulations we assigned half the host cells of either F^- or Hfr to be immune, keeping total initial host density at our standard value. These immune colonies contribute to a phage loss proportional to both their density and radius. For standard density the host number in each colony reaches about 1500, reflecting growth of 2×10^6 hosts/ml to an assumed carrying capacity of 3×10^9 bacteria/ml.

G. *In silico* infections

Figure 5 illustrates the simulated development of the F^- strain in a mixed lawn of 91% F^- and 9% Hfr following infection. In initial experiments we found a 10:1 ratio of F^- to Hfr was necessary to give a visible GFP signal. The mixed population was infected with either the λ or the M13 form of λS3243 and allowed to grow until the nutrients were depleted. As the great majority of GFP fluorescence came from infected F^- bacteria (Fig. 2), we show here only the corresponding density of the infected F^- strain. The 24-hour value of each curve simulates an experimental measurement. The figure shows simulations for the full system, some variants, and situations where one or the other of the *E. coli* hosts cannot develop progeny phages.

The requirement of a tenfold difference in the ratio of the two strains may be due to the relative burst sizes of the two infections. The F^- produced few M13-form progeny while the Hfr produced many λ-form progeny. The starting concentration of all bacteria is 2×10^6/ml when counting volume of both top and bottom agar in a spot. Although the bacteria are limited to the soft agar or the upper 10% of the column volume, the total volume in a spot defines the carrying capacity because the bottom agar provides the nutrients. We simulated the effect of this separation by adjusting the equations with 11 times higher η values than in Table II but with densities and carrying capacity as if the entire column volume was available. That is, not only are nutrients from the entire column volume assumed to be available but phages are assumed to be lost when entering the bottom agar. Notice that the grey curve in Fig. 5 represents the population of uninfected F^- bacteria, thereby giving an overall scale for the signal.

1. Calibration of model: Single-round experiments

The simulation parameters are taken from Table II, where the expected diffusive loss from the 0.7 mm top agar to the bottom agar is about 1/650 min (assuming a diffusion constant of 6.2 $\mu m^2/s$ reported for phage λ [21]). D was measured to 7 $\mu m^2/s$ for the filamentous phage fNEL of length 1.4 μm [22], and we accordingly chose the same loss term for the two phage forms.

Figure 3(b) illustrates that single-round infections of the F^- strain required about 1000 times as many phages to cause

TABLE II. Model parameters used in the *in silico* model of the considered two-host *in vivo* model of a vector-borne disease. Bacterial growth was monitored by A600 after dilution to the linear range of our spectrophotometer. A density of 10^8 cells/ml by counting bacteria with a Petroff-Hausser chamber generated an A600 of 0.18. We further measured growth of the infected F^- strain, S3247, and found that it was the same as the uninfected strain. The curing rate of infected F^-, $0.8\Gamma_f$ or 55% per host generation, is substantially larger than the 10% per generation reported for wild-type M13 [18]. High curing rate is needed to reproduce the inefficient final infection of F^- in single-round experiments [Fig. 3(b)]. The factor 1/2 in Ω_m is included because half the M13-form phages produced by an F^- colony are expected to be lost by secretion into the colony.

Parameter	Meaning	Value	Source
Γ_f	Growth rate (F^-)	ln(2)/(72 min)	Fig. 4(a)
Γ_{cure}	Loss of infectivity	$0.8\Gamma_f$	Fit to Fig. 2(b)
Γ	Growth rate (Hfr)	ln(2)/(64min)	Fig. 4(b)
K	Carrying capacity	3.1×10^9/ml	Saturated broth culture
f_0	Initial F^-	1.6×10^5/ml	Measured
v_0	Initial Hfr	1.6×10^6/ml	Measured
η_λ	Adsorption of λ	0.65/min/(10^9/ml)	From Ref. [19]
η_m	Adsorption of M13	0.09/min/(10^9/ml)	From Ref. [20]
$Loss_\lambda$	Loss of λ phage	1/(650 min)	Loss from 0.9 mm with 6.2 μm^2/s diffusion
$Loss_m$	Loss of M13 phage	1/(650 min)	Estimated as $Loss_\lambda$
Ω_m	Production of M13	0.040/min×0.5	Fig. 4(c)
τ_m	Latency time (M13)	130 min	Fig. 4(c)
k_m	Latency form factor	3	Fig. 4(c)
β	Burst of λ	70	Fig. 4(d)
τ_λ	Latency time (λ)	150 min	Fig. 4(d)
k_λ	Latency form factor	10	Fig. 4(d)

similar low GFP signal as the multiple rounds of infections shown in Fig. 3(a). The 10^7 PFU for single-round propagation corresponds to a multiplicity of infection of about 50 and should accordingly give a much larger final GFP signal if the initially infected F^- were maintaining their infections throughout the experiment. Introducing a curing rate Γ_{cure} of $0.8\Gamma_f$ allowed us to approximately match the single-round experiment with 10^7 λ-form PFU to 10^4 λ-form PFU in the multiple-round experiments. This curing further predicts a slightly weaker GFP signal when using 10^4 M13-form PFU in the multiple-round experiment (solid red curve). The predicted accumulation of GFP from single-round M13 infection does not match the experiment in Fig. 3(c) because the infected KS5 strain is producing less GFP than the infected S3247.

We have also attempted to reproduce the experiment with a simpler well-mixed version of our model. This is obtained by setting $f_{\text{coll}} = f$, $f_{\text{coll-all}} = f + f^L + f^*$, $v_{\text{coll}} = v$, and $v_{\text{coll-all}} = v + v^L$. In that case a moderate fit to Fig. 3 requires tenfold lower adsorption rates of both phages, and also a tenfold higher loss rate of phage λ. This points to the fact that a well-mixed model grossly overestimates the availability of hosts for infection, and requires unrealistically "weak" phages for reproducing the observed results.

2. *Predictions and test: Colony sizes*

Figure 5(b) shows four infection trajectories that all are initiated with a spot of 7×10^5 phages distributed above a volume of approximately 0.7 cm^3 [as experiment in Fig. 2(a)]. The green area and lines correspond to infections initiated with the λ form, while the red curves correspond to infections initiated with the M13 form. Dashed curves show development of single-cycle infections. In our model multiple cycles of infection only exceed the yield of single-cycle infections after about 6–8 hours, reflecting long latency times and slow adsorption when host densities are low.

Figure 5(b) also illustrates a simulation where the initial bacteria density is reduced by a factor of 10. This results in about the same final total number of bacteria, but distributed in tenfold-larger colonies. Thus, the typical colony sizes change from about 1500 to about 15 000. The prediction of our colony-based model is that these larger colonies delay transmission of the phages. The dark green curve in the figure shows the model predicts about a factor-of-10 reduction in total final infected F^- hosts, compared to the case with smaller colonies.

To test the above prediction we infected a tenfold diluted version of our mixed culture. To make a quantitative prediction we measured the lowest phage inoculum that allowed us to detect a final GFP signal, and we do this both with standard and changed density of hosts in the lawn. Starting with a concentration of 10^7 PFU/ml, the phage concentration was serially diluted threefold before spotting on the bacteria except in an initial M13-form experiment where the phages were serially diluted tenfold before spotting. Care was taken that the green channel was free of saturated pixels and the average grayscale value of pixels adjacent to the spot was subtracted from the average grayscale value within the spot to quantify the fluorescence. The limit of detection was defined as when the fluorescence fell to below half the higher concentrations. The resolution in Table III is limited by the threefold dilution between the PFU steps. We made the measurements independently several times, reported by different colors in Table III.

TABLE III. Initial phage infection needed to cause a detectable GFP signal. Colors indicate independent repeats of the measurements. Higher numbers imply a correspondingly weaker infection propagation. The top portion of the table varied the initial bacterial density, in factors of the basic level $B_0 = 2 \times 10^6$/ml (partitioned in 91% F^- and 9% Hfr). The lower portion of the table assigns 50% of host bacteria of one strain to be immune. If the F^- was 50% immune, KS5 replaced half of S3247. If the Hfr was 50% immune, KS3 replaced half of S3253. The ratio in column 3 is obtained by dividing the observed threshold with the corresponding value without immune fraction. The "Ratio model" in column 4 shows the predictions of our model using the measured relative growth rates of the F^- strains, KS5 and S3247. KS5 grows approximately 25% faster than normal S3247 (Supplemental Material Fig. S4 [13]). Assuming equal growth rates for KS5 and S3247, the "Ratio model" predicts only 6.6- and 5-fold effects for infections by the λ and M13 forms, respectively (instead of 50- and 40-fold shown above when measured growth rates were considered).

Bacterial density		Ratio data	Ratio model
	λ-form PFU per spot		
×0.1	3.7×10^5, 1.2×10^5	9	12
×1	4.1×10^4, 1.4×10^4	1	1
×10	1.4×10^4, 4.6×10^3	0.3	0.7
	M13-form PFU per spot		
×0.1	1.0×10^7, 3.3×10^6	18	25
×1	3.7×10^5, 3.7×10^5	1	1
×10	4.1×10^4, 4.1×10^4	0.1	0.3
Immune Strain (50%)	λ-form PFU per spot		
none	4.1×10^4, 4.1×10^4, 4.1×10^4	1	1
F^-	3.3×10^6, 1.1×10^6, 1.1×10^6	45	50
Hfr	1.2×10^5, 4.1×10^4, 1.2×10^5	2.3	3.3
	M13-form PFU per spot		
none	3.7×10^5, 1.0×10^5	1	1
F^-	1.0×10^7, 1.0×10^7	63	40
Hfr	1.1×10^6, 1.0×10^5	2	5

The third column in Table III shows the ratio of the initial phage inoculum to reach the threshold level of detected GFP under the given condition compared with the number of phages used under standard conditions:

$$\text{Ratio} = \frac{\text{phage (Initial bacteria } = 0.1 \times \text{standard)}}{\text{phage (Initial bacteria } = \text{ standard)}}.$$

This ratio was used to quantify the efficiency of phage propagation. The lawn initiated with diluted bacteria required a ninefold-higher initial λ-form phage density to produce the same final GFP fluorescence as observed with the standard lawn initiated with 1.2×10^6/ml F^- and 1.2×10^5/ml Hfr. This means the infection was effectively reduced by a factor of 9 due to formation of ten times larger colonies. Noticeably, an increased density of the bacteria had a less pronounced effect, as a tenfold-larger initial host density only causes a $1/0.3 = 3$-fold increase in infection spreading.

In the simulation the above ratio is measured by changing initial phage load until the obtained f^* just reaches 10^7/ml. The model predictions for the ratio in Table III are independent of the choice of this arbitrary threshold. The table shows that the model for colony-based propagation closely matches the experimentally measured ratios, both for small and large colonies and in particular for the increased effect of colony structure when we initiate the infection by M13 form instead of the λ form.

3. Predictions and test: Partial immunization

The experimental system also allowed us to consider mitigation of epidemic spreading. To do this we considered partial immunization; strains in the initial lawn were partly replaced by immune hosts of either F^- (KS5) or Hfr (KS3). In this case we fixed the total initial host density in the mixed lawn to the standard value. The lower part of Table III quantified the effect of replacing 50% of the S3247 with KS5, or replacing 50% of S3253 with KS3. We observed a substantial effect with the F^-, while the effect of Hfr immunization was much weaker. The model predictions for immunizations are within the experimental accuracy.

Initially, our model underestimated the large effect of immunizing half of the F^- population. This disagreement between the model and the experiment led us to examine the growth rates of S3247 and KS5. We replicated the growth conditions at the start of the infections and found KS5 grew 25% faster than S3247 (see Supplemental Material Fig. S4 [13]). Incorporating the growth rate difference allowed our model predictions to match the experiment within the resolution of our experimental data (Table III).

An interesting aspect of this system is that the two hosts showed different sensitivity to partial immunization. By analogy with a malaria epidemic, immunizing F^- could correspond to a vaccination of half the human population. Immunizing Hfr or reducing Hfr could correspond to a strategy of partly draining a swamp inhabited by a disease-transmitting mosquito.

III. DISCUSSION

We developed a model system for the spread of a vector-borne disease using nonhazardous surrogates. The model system integrates experiments with an *in silico* model. The experimental system relies on a derivative of the bacterial virus, bacteriophage λ, with a life cycle that requires two hosts. We quantified the growth properties of the phage and hosts and examined the spread of the phage where the two bacterial hosts grow as independent microcolonies. We also developed an *in silico* model that described the spread of the phage within and between the microcolonies or bacterial communities. Furthermore, we experimentally tested the *in silico* model and observed the predicted dependence on the distance between colonies and the effect of partial immunization or herd immunity.

The *in silico* model extends standard models for well-mixed phage-bacteria systems [23–26] with the more difficult host location associated with colony formation [16]. The model was simplified by ignoring spatial fluctuations and assuming both susceptible and already-infected hosts were randomly mixed at the surface of each colony. All parameters were experimentally determined, with the curing rate

of infected F^- adjusted to reproduce experimentally obtained ratios of F^- infected hosts in single- and multiple-round experiments. The model and experiment quantified the extent that virus propagation in the agar gel was reduced when each replication required diffusion to a new host colony. The predicted effect of colony formation was confirmed experimentally by varying the initial concentration of bacteria (Table III).

In the language of the vector-borne disease, malaria, immunizing of F^- would correspond to either vaccinating humans or adding animals that the mosquito may infect but which do not allow for transmission back to another mosquito. This last mechanism possibly reduced malaria in northern Europe [27] and the USA [28] more than a century ago.

This model of a vector-borne epidemic permitted exploration of disease propagation and mitigation strategies. Examples were explored in Table III which considered the effect of separating hosts into more spatially segregated communities, and on immunizing (vaccinating) half of one of the hosts against transmitting the disease. We learned that spatial organization had a clear effect, with larger separation leading to much less disease spreading. In fact about a factor-of-10 reduction in infections was obtained by a twofold increase in the distance between the two host types. We also found that a twofold reduction in the fraction of either of the two hosts able to propagate the phage led to less infection of F^-. The results of both tests are shown in Table III. Thus, we have developed an integrated model system for vector-borne disease that may easily be adopted to test mitigation strategies in terms of immunization and changed spatial organization of one or both host types.

Our model system has quite different infection parameters than real vector-borne diseases. The latency time and propagation of the disease take place on timescales of bacterial generations, while vector-borne diseases have spreading dynamics that are much faster than the generation time of humans. This means that accurate modeling of our system was needed in order to allow generalization to parameters for more realistic scenarios of humans and their counterparts in a particular vector-borne disease. Furthermore, infection of our immune strain, KS5, produced a weaker GFP signal [Figs. 3(c) and 3(d) vs Fig. 3(b)] than from infection of the productive strain, S3247. The difference in GFP production could in part be due to a higher copy number of the infecting S3243 in the presence of the M13 helper plasmid. We ignored this difference in our analysis of disease spreading.

The model worked remarkably well, in spite of ignoring spatial fluctuations that could occur as rare early infections of especially the minority strain Hfr create hot spots for infection between particularly close F^- and Hfr colonies. This may also serve as an explanation for the marginally smaller effect of 50% immunization of the Hfr strain in the experiment (2–2.3) compared to the model (3.3–5): With 50% immune Hfr colonies there would be twofold fewer infectious pairs of close colonies, with subsequent rounds of infection acting primarily between the fully infectious pairs.

Our two-host phage propagation system presents a nontraditional way to mimic outbreaks of a vector-borne disease. It differs in a number of ways from what we would expect in an eventual epidemic involving humans. As pointed out above, the phages have a latency that is longer than the lifetimes of hosts, while the exposed state in vector-borne diseases is of the order of weeks and thus much shorter than a human lifetime. Furthermore, our experimental setup is a batch culture and thus limited to a few rounds of infection. This last limitation may be lifted by considering continuous flow systems, for example, using a microfluidics system [29–31]. This would also allow us to study both the microscopic spreading pattern and the impact of different spatial organizations.

We would like to point out some other features of vector-borne disease that could be examined by the dimorphic phage system. An obvious one is the role of mosquito magnets. That is, a subpopulation of hosts is bitten more frequently [32] and this subpopulation has a greater probability of spreading disease (for example, [33]). In our system, would a subset of sensitive, hyper-infectable host bacteria counter the reduction in spread by an immune subpopulation? Conversely, would hyper-infectable immune hosts protect sensitive hosts better? Mosquito magnets are becoming more easily identifiable [34,35]. In the case of limiting the availability of vaccines or future antimalarial prophylaxis, could the gains of treating mosquito magnets first be quantified?

Seen from a greater perspective, our construct has peculiarities and limitations. However, normal diseases will also greatly differ from each other in their spreading pattern: Some will be endemic, and others epidemic, and some will have alternating infection entries into their host (bubonic versus pneumonic plaque) while others will be dominated by superspreaders [36] facilitated by, for example, mosquito magnets. Some of these features can be implemented in our construct and used to think about vector-borne disease spreading in a wider perspective than provided by already established models [37].

IV. MATERIALS AND METHODS

A. Bacterial genotypes and construction of λS3243

Detailed construction of λS3243 and its preparation as λ and M13 forms are described in the Supplemental Material [13]. The λ form was induced from a lysogen of HO480 [38]. Contaminating λ form was removed from preparations of the M13 form by heat inactivation [39,40].

Genotypes of all *E. coli* strains used in this study are described in Table I of the Supplemental Material [13]. Other than HO480, all F^- strains were derived from MC4100 [41]. All the Hfr strains were derived from S971 [42]. The defective λ prophage in KS5, S3207, S3208, S3247, and S3248 is described in [43]. pSB4423 is an M13 helper plasmid [10] and pACYC184 [44] is the parental vector plasmid of pSB4423.

Our original motivation in preparing λS3243 was to improve yield and simplify the preparation of large scaffolds for DNA origami [10,11]. After constructing λS3243 a survey of growth media identified conditions for improved yield and could bypass the requirement for phage purification by isopycnic centrifugation.

The dimorphic phage λS3243 was derived from λ*cI857 nin5* and harbors a 2275-base-pair M13 phagemid, pIO13, inserted into its XbaI site. pIO13 is pSB4434 [45] with the insertion of a p*tac-gfpmut2* [46] fusion. The IG region of pIO13 was derived from the M13-related bacteriophage, f1, and directs DNA synthesis and packaging by M13 proteins [9]. The initial clone of λS3243 was selected as a lysogen of HO480 resistant to 50 μg/ml ampicillin at 30 °C. The orientation of the inserted phagemid was determined by PCR. λS3243 packages the standard map of λ into M13 in the 5′-3′ orientation. A second dimorphic phage, λS3242, bears pIO13 in the opposite orientation. λS3242 packages the standard map of λ into M13 in the 3′-5′ orientation. λS3242 produced spots with less fluorescence than λS3243 and was not characterized further in this study.

B. Spot tests, method

Log-phase cultures were established in Yeast Extract Tryptone medium (YT) [47] supplemented with 15 μg/ml chloramphenicol at 37 °C. Our standard inoculum used 1.1×10^8 F^- cells and 1.1×10^7 Hfr cells in less than 1 ml YT broth. The mixed cultures were diluted with 3 ml molten F-top [47] and cast over MC agar ([48,49] and Supplemental Material [13]). After the soft agar overlay gelled, 10 μl samples of phages in a modified Tris-magnesium gelatin (TMG) buffer ([50] and Supplemental Material [13]) were spotted on the soft agar. Spots were allowed to soak into the agar at room temperature and the Petri dishes were incubated overnight at 37 °C.

Note added in proof. The DNA sequence of lambdaS3243 is on GenBank with accession number OR474059.

ACKNOWLEDGMENTS

We thank Thom LaBean, Namiko Mitarai, and Steen Pedersen for helpful discussions. This work was supported by the European Research Council (ERC) under the European Union's Horizon 2020 research innovation program, Grant Agreement No. 740704, and by a grant from the Danish National Research Foundation (Grant No. DNRF170) through the Center of Excellence PANDEMIX.

The authors declare no competing interests.

[1] World Health Organization, Vector-borne diseases, https://www.who.int/news-room/fact-sheets/detail/vector-borne-diseases (2020).

[2] A. Steere, J. Coburn, and L. Glickstein, The emergence of Lyme disease, J. Clin. Invest. **113**, 1093 (2004).

[3] F. Sanger, A. Coulson, G. Hong, D. Hill, and G. Petersen, Nucleotide sequence of bacteriophage lambda DNA, J. Mol. Biol. **162**, 729 (1982).

[4] M. Hofnung, D. Hatfield, and M. Schwartz, *malB* region in *Escherichia coli* K-12: Characterization of new mutations, J. Bacteriol. **117**, 40 (1974).

[5] M. Schwartz and L. Le Minor, Occurrence of the bacteriophage λ receptor in some enterobacteriaceae, J. Virol. **15**, 679 (1975).

[6] P. van Wezenbeek, T. Hulsebos, and J. G. G. Schoenmakers, Nucleotide sequence of the filamentous bacteriophage M13 DNA genome: Comparison with phage fd, Gene **11**, 129 (1980).

[7] D. Marvin, M. Symmons, and S. Straus, Structure and assembly of filamentous bacteriophages, Prog. Biophys. Mol. Biol. **114**, 80 (2014).

[8] A. Oppenheim, O. Kobiler, J. Stavans, D. Court, and S. Adhya, Switches in bacteriophage λ development, Annu. Rev. Genet. **39**, 409 (2005).

[9] G. Dotto, V. Enea, and H. Zinder, Functional analysis of bacteriophage f1 intergenic region, Virology **114**, 463 (1981).

[10] A. Marchi, I. Saaem, B. Vogen, S. Brown, and T. LaBean, Toward larger DNA origami, Nano Lett. **14**, 5740 (2014).

[11] P. Rothemund, Folding DNA to create nanoscale shapes and patterns, Nature (London) **440**, 297 (2006).

[12] J. Cleary and D. Ray, Replication of the plasmid pBR322 under the control of a cloned replication origin from the single-stranded DNA phage M13, Proc. Natl. Acad. Sci. USA **77**, 4638 (1980).

[13] See Supplemental Material at http://link.aps.org/supplemental/10.1103/PRXLife.1.013015 for detailed descriptions of methods used to prepare reagents used in this paper, physical analyses of the M13 form, Figs. S1–S4, and Supplemental Table 1. Supplemental Fig. S5 illustrates aspects of the model.

[14] W. Salivar, H. Tzagoloff, and D. Pratt, Some physical-chemical and biological properties of the rod-shaped coliphage M13, Virology **24**, 359 (1964).

[15] K. Yamamoto, B. Alberts, R. Benzinger, L. Lawhorne, and G. Treiber, Rapid bacteriophage sedimentation in the presence of polyethylene glycol and its application to large-scale virus purification, Virology **40**, 734 (1970).

[16] R. Eriksen, N. Mitarai, and K. Sneppen, Sustainability of spatially distributed bacteria-phage systems, Sci. Rep. **10**, 3154 (2020).

[17] S. Cohen and A. Chang, Genetic expression in bacteriophage lambda. 3. Inhibition of *Escherichia coli* nucleic acid and protein synthesis during lambda development, J. Mol. Biol. **49**, 557 (1970).

[18] V. Merriam, Stability of the carrier state in bacteriophage M13-infected cells, J. Virol. **21**, 880 (1977).

[19] S. Brown, N. Mitarai, and K. Sneppen, Protection of bacteriophage-sensitive *Escherichia coli* by lysogens, Proc. Natl. Acad. Sci. USA **119**, e2106005119 (2022).

[20] M. De Paepe and F. Taddei, Viruses' life history: Towards a mechanistic basis of a trade-off between survival and reproduction among phages, PLoS Biol. **4**, e193 (2006).

[21] R. Moldovan, E. Chapman-McQuiston, and X. Wu, On kinetics of phage adsorption, Biophys. J. **93**, 303 (2007).

[22] J. Hu, K. Miyanaga, and Y. Tanji, Diffusion properties of bacteriophages through agarose gel membrane, Biotechnol. Progr. **26**, 1213 (2010).

[23] A. Campbell, Conditions for the existence of bacteriophage, Evolution **15**, 153 (1961).

[24] B. Levin, F. Stewart, and L. Chao, Resource-limited growth, competition, and predation: A model and experimental studies with bacteria and bacteriophage, Am. Nat. **111**, 3 (1977).

[25] T. Thingstad, Elements of a theory for the mechanisms controlling abundance, diversity, and biogeochemical role of lytic bacterial viruses in aquatic systems, Limnol. Oceanogr. **45**, 1320 (2000).

[26] J. Weitz, Quantitative viral ecology, in *Quantitative Viral Ecology* (Princeton University Press, Princeton, NJ, 2016).

[27] A. Hamoudi and J. Sachs, The changing global distribution of malaria: A review, CID Working Paper No. 2 (1999), Center for International Development Harvard University.

[28] L. Williams, Jr., Malaria eradication in the United States, Am. J. Public Health Nations Health **53**, 17 (1963).

[29] F. Hol and C. Dekker, Zooming in to see the bigger picture: Microfluidic and nanofabrication tools to study bacteria, Science **346**, 1251821 (2014).

[30] S. Taheri-Araghi, S. Bradde, J. T. Sauls, N. S. Hill, P. A. Levin, J. Paulsson, M. Vergassola, and S. Jun, Cell-size control and homeostasis in bacteria, Curr. Biol. **25**, 385 (2015).

[31] A. Sidi Mabrouk, V. Ongenae, D. Claessen, S. Brenzinger, and A. Briegel, A flexible and efficient microfluidics platform for the characterization and isolation of novel bacteriophages, Appl. Environ. Microbiol. **89**, e01596-22 (2023).

[32] R. Muirhead-Thomson, The distribution of anopheline mosquito bites among different age groups, BMJ **1**, 1114 (1951).

[33] D. Smith, F. McKenzie, R. Snow, and S. Hay, Revisiting the basic reproductive number for malaria and its implications for malaria control, PLoS Biol. **5**, e42 (2007).

[34] M. De Obaldia, T. Morita, L. Dedmon, D. Boehlmer, C. Jiang, E. Zeldon, J. Cross, and L. Vosshall, Differential mosquito attraction to humans is associated with skin-derived carboxylic acid levels, Cell **185**, 4099 (2022).

[35] D. Giraldo, S. Rankin-Turner, A. Corver, G. Tauxe, A. Gao, D. Jackson, L. Simubali, C. Book, J. Stevenson, P. Thuma, R. McCoy, A. Gordus, M. Mburu, E. Simulundu, and C. McMeniman, Human scent guides mosquito thermotaxis and host selection under naturalistic conditions, Curr. Biol. **33**, 2367 (2023).

[36] A. Teicher, Super-spreaders: A historical review, Lancet Infect. Dis. (2023), doi: 10.1016/S1473-3099(23)00183-4.

[37] S. Mandal, R. R. Sarkar, and S. Sinha, Mathematical models of malaria: A review, Malar. J. **10**, 202 (2011).

[38] B. Hove-Jensen, Two-step method for curing *Escherichia coli* of ColE1-derived plasmids, J. Microbiol. Methods **72**, 208 (2008).

[39] J. Rider, A. Sparks, N. Adey, and B. Kay, Microbiological methods, in *Phage Display of Peptides and Proteins: A Laboratory Manual* (Academic Press, San Diego, CA 1996), pp. 55–65.

[40] E. Rossomando and H. Bladen, Physical changes associated with heating bacteriophage f1, Virology **39**, 921 (1969).

[41] M. Casadaban, Transposition and fusion of the *lac* genes to selected promoters in *Escherichia coli* using bacteriophage λ and mu, J. Mol. Biol. **104**, 541 (1976).

[42] S. Brown, Mutations in the gene for EF-G reduce the requirement for 4.5S RNA in the growth of *E. coli*, Cell **49**, 825 (1987).

[43] K. Bæk, S. Svenningsen, H. Eisen, K. Sneppen, and S. Brown, Single-cell analysis of λ immunity regulation, J. Mol. Biol. **334**, 363 (2003).

[44] A. Chang and S. Cohen, Construction and characterization of amplifiable multicopy DNA cloning vehicles derived from the P15A cryptic miniplasmid, J. Bacteriol. **134**, 1141 (1978).

[45] S. Brown, J. Majikes, A. Martínez, T. Giron, E. C. Fennell, and T. LaBean, An easy-to-prepare mini-scaffold for DNA origami, Nanoscale **7**, 16621 (2015).

[46] B. Cormack, R. Valdivia, and S. Falkow, FACS-optimized mutants of the green fluorescent protein (GFP), Gene **173**, 33 (1996).

[47] J. Miller, *Experiments in Molecular Genetics* (Cold Spring Harbour Laboratory Press, New York, 1972).

[48] A. Pardee, F. Jacob, and J. Monod, The genetic control and cytoplasmic expression of "inducibility" in the synthesis of β-galactosidase by *E. coli*, J. Mol. Biol. **1**, 165 (1959).

[49] K. Norregaard, M. Andersson, P. Nielsen, S. Brown, and L. Oddershede, Tethered particle analysis of supercoiled circular DNA using peptide nucleic acid handles, Nat. Protoc. **9**, 2206 (2014).

[50] J. Little, D. Shepley, and D. Wert, Robustness of a gene regulatory circuit, EMBO J. **18**, 4299 (1999).